The Astrophysical Journal, 686:310–324, 2008 October 10


# THE STELLAR POPULATION OF M17[1]

V. H. Hoffmeister, R. Chini, C. M. Scheyda, D. Schulze, and R. Watermann
Astronomisches Institut, Ruhr–Universität Bochum, 44780 Bochum, Germany

D. Nürnberger
European Southern Observatory, Casilla 19001, Santiago 19, Chile

and

N. Vogt[2]
Departamento de Física y Astronomía, Universidad de Valparaíso, Valparaíso, Chile
*Received 2007 December 19; accepted 2008 June 10*

## ABSTRACT

The stellar content of M17 has been investigated by multicolor photometry and spectroscopy. Various independent estimates yield a distance of 2.1 $\pm$ 0.2 kpc. The ratio of total-to-selective extinction is $R = 3.9$. Within a projected area of $3.6 \times 3.7$ pc, there are several thousand stars. About 74% of them show infrared excess suggesting the presence of dense circumstellar material; the excess frequency is higher for fainter stars. The number of spectroscopically classified exciting stars could be enlarged from 13 to 46. The two central O4 stars are both spectroscopic binaries; multiplicity of other early O-type stars could also be established, increasing the number of high-mass stars even further. Our data suggest at least two episodes of star formation: There are about 500 ZAMS sources ($2 < A_V < 7$)—among them many spectroscopically classified OB stars and a significant fraction of lower mass sources with infrared excess ($\sim$25%) and X-ray emission ($\sim$6%). About 3350 heavily reddened sources with $10 < A_V < 40$) are most likely deeply embedded pre-main-sequence objects with an age of less than $5 \times 10^5$ yr. This group contains about 47% sources with infrared excess and 12% X-ray emitters. Cluster members later than about A0 have not yet reached the main sequence. In addition, a group of 647 protostellar candidates ($1.5 < K - L < 6.9$) has been detected in the cluster center as well as in the northern and southwestern bar. This population of accreting protostars argues in favor of ongoing star formation triggered by the central O stars in M17.

*Subject headings:* dust, extinction — H ii regions — infrared: stars — open clusters and associations: individual (M17, NGC 6618) — stars: early-type

*Online material:* color figures

## 1. INTRODUCTION

M17 is one of the most prominent H ii regions in our Galaxy and associated with molecular clouds to the north and to the southwest. Due to the heavy obscuration by dust, the radio peak is displaced about 4′ to the west of the maximum H$\alpha$ emission. This has led to the suggestion of a blister model in which the H ii region is eating into the southwestern molecular cloud. The large extinction in that area is also the reason why only limited information about the stellar content of M17 could be obtained for many decades. Schulte (1956) classified the first early-type star in the region spectroscopically as O5; this was confirmed later by Anderson (1970). A second early-type star was classified as B0 (Pronik 1958), OB$^+$ (Stephenson & Hobbs 1961), and finally as O8.5 V (Crampton et al. 1978). Kleinmann (1973) observed a third early-type star, which he described as "double O or early B." Meanwhile, there are some survey-type studies of the embedded young cluster both in the optical/infrared (IR) and the X-ray regime.

### 1.1. *Optical Surveys*

Ogura & Ishida (1976) presented *UBV* photometry for about 700 stars in a $30' \times 30'$ field centered at the radio position of M17. Using low-dispersion spectra, they found six heavily reddened O- or possible O-type stars embedded in the central part of the H ii region. The first evidence for a young embedded cluster came from Beetz et al. (1976), who found more than 100 partly heavily obscured stars within a circular field of 4′ diameter by means of *R*- and *I*-band imaging. Subsequently, Chini et al. (1980, hereafter CEN80) investigated this cluster by *UBVRI* photometry and classified six O-type stars (O4–O9) to account for both the ionization and the IR luminosity of the H ii region. The major exciting star was a double O4-type (CEN 1) located in the cluster center at R.A. = $18^{\rm h}20^{\rm m}29.9^{\rm s}$ and decl. = $-16°10'45''$ (J2000.0) and is identical to Kleinmann's anonymous double star; this central position has been used for all subsequent cluster studies. In addition, CEN80 presented the first evidence for a higher than normal ratio of total to selective extinction in the region. Since then no further attempts have been made to study the cluster at optical wavelengths.

### 1.2. *X-Ray Sources*

Broos et al. (2007) observed the stellar populations of M17 in a $17' \times 17'$ field centered on CEN 1 with *Chandra* (ACIS). The field reveals 886 sources with observed X-ray luminosities in the range $\sim$29.3 ergs s$^{-1}$ $< \log L_{\rm X} <$ 32.8 ergs s$^{-1}$. Broos et al. described the X-ray properties of 33 known OB stars, which corroborate the correlation between X-ray and bolometric luminosities of $L_{\rm X} \sim 10^{-7} L_{\rm bol}$. From this list 12 O and 19 B0–B3 stars were previously identified by CEN80 while two additional O stars have

[1] Based on observations collected at the European Southern Observatory, Chile, Programs 069.C-0303(A), 071.D-0084, 073.C-0170(A+B), 075.C-0381(A+B), and 077.C-0291(A+B).

[2] Instituto de Astronomía, Universidad Católica del Norte, Antofagasta, Chile.

been detected before by Ogura & Ishida. On the other hand, 15 B0–B3 stars from the compilation by CEN80 have no X-ray counterparts, which may be partly due to low-quality photometric spectral types in the work by CEN80. Broos et al. (2007) presented a list of 114 new photometrically selected intermediate- and high-mass candidates (>2 $M_{\odot}$).

### 1.3. *Infrared Surveys*

Lada et al. (1991) performed first *JHK* imaging of a field of $9' \times 9'$ centered on CEN 1. Adopting a distance of 2.2 kpc and a visual extinction of 5–10 mag for cluster members Lada et al. identified more than 100 OB stars clustering in the obscured portion of the H II region of several parsecs in diameter. In addition, most OB stars were found to have *K*-band excess. Giard et al. (1994) presented *K*- and *L*-band images of the southwestern interface of the H II region with the molecular cloud with a focus on the interstellar dust grains. As a by-product they listed seven extremely red objects ($K - L > 3.4$) which were interpreted as young stars in a very early evolutionary stage. Hanson et al. (1997) presented positions for 355 IR objects within a $6' \times 6.2'$ field centered onto CEN 1. Their multiwavelength spectroscopic survey of 13 known OB star candidates in the cluster corroborated and/or improved the existing spectral-type designations. Nielbock et al. (2001) concentrated on the circumstellar environment of some of these high-mass stars presenting 10 and 20 $\mu$m imaging of the area. The SEDs and the morphology of the MIR emission strongly suggested that some OB stars are surrounded by circumstellar dust. Jiang et al. (2002) conducted an extensive *JHK* survey covering an area of $\sim 14' \times 14'$. Using a distance of 1.6 kpc they interpreted the IR color-magnitude diagram as to be composed of a congregation of intermediate- to high-mass stars in the central region surrounded by a second generation of younger stars in the nebular bars. A low-resolution (5.6″) *JKL* survey by Ando et al. (2002) covered a region of $20' \times 20'$ and revealed 38 sources brighter than 7 mag at 3.67 $\mu$m; among them were the 13 known OB stars.

### 1.4. *Distance*

The distance of M17—one of the nearest giant H II regions in the Galaxy—is still under debate, with values ranging from 1.3 to 2.9 kpc. Ogura & Ishida (1976) performed spectrophotometric observations of 51 stars with fairly low reddening (only 7 stars in their study have $A_V > 3$ mag) and found a distance of 1.3 kpc. CEN80 derived a distance of $2.2 \pm 0.2$ kpc based on *UBV* photometry of 19 possible early-type stars. Nielbock et al. (2001) readdressed this distance determination by excluding IR excess objects from the sample of CEN80 and by using an extinction law with $R = 4.8$. From 16 early-type stars a mean distance of $1.6 \pm 0.3$ kpc was obtained. Hanson et al. (1997) used spectra and *K*-band magnitudes of five O-type stars to determine a distance of $1.3^{+0.4}_{-0.2}$ kpc. Russeil (2003) obtained a kinematic distance of 2.4 kpc from radio data. A recent distance estimate of $1.6^{+0.3}_{-0.1}$ kpc was obtained by balancing the integrated flux in the observed spectral energy distribution (SED) of the H II region with the total bolometric luminosity of all known O and early B stars in the cluster (Povich et al. 2007).

### 1.5. *Reddening Law*

Higher than normal ratios of total to selective extinction, i.e., $R = A_V/E_{B-V} > 3.1$, are theoretically expected due to grain growth in dense clouds, as discussed, e.g., by Chini & Krügel (1983) or Cardelli et al. (1989). CEN80 interpreted their photometric *UBVRI* results as due to an abnormal reddening law in M17, characterized by $R = 4.2$. Chini & Wargau (1998) have extended the observed wavelength range up to 4.8 $\mu$m and derived an even larger *R*-value of 4.8 from various color-color diagrams. Hanson et al. (1997) determined individual *R*-values for 12 OB stars in M17 by fitting dereddened SEDs to model atmospheres; they found a range of $2.8 \leq R \leq 5.5$ with an average of $R = 4.1$, corroborating the earlier results by CEN80 concerning the high ratio of total to selective extinction.

### 1.6. *Outline of the Paper*

The goal of this paper is to explore the stellar population in M17 by multiwavelengths photometry and spectroscopy with unprecedented spatial resolution and sensitivity. Our data comprise an area that mainly covers the embedded cluster as observed by CEN80 and part of the southwestern molecular cloud where ongoing star formation is expected. After the presentation of the observations and results in § 2, we take a closer look at the reddening law of the region in § 3. Given the large range of distances for M17 in the literature a new determination seems highly desirable; in § 4 we present three independent methods. Next, in § 5, we investigate general cluster properties, including the search for further embedded exciting sources as well as the study of the fairly unknown pre-main-sequence (PMS) population. We discuss the age of the cluster and the disk frequency. Finally, § 6 deals with the proposed scenario of sequential star formation in the M17 region.

## 2. OBSERVATIONS AND RESULTS

### 2.1. *Imaging*

We have performed *BVRI* imaging with ESO New Technology Telescope (NTT) and EMMI (Dekker et al. 1986) in 2003 July. The central position was R.A. = $18^{h}20^{m}28.9^{s}$, decl. = $-16°10'30''$, with a field of view of $10' \times 10'$. All images have been obtained with *B*b, *V*, and Gunn *r* and *i* filters. The pixel resolution and the effective spatial resolution was 0.33″ and 1.1″ (FWHM), respectively. To cover a large range in stellar brightness various integration times have been used (*B*b: 10, 300 s; *V*: 5, 300 s; *r*: 3, 20, 300 s; *i*: 2, 20, 300 s). However, a few of the brightest sources are still saturated. The photometrically calibration has been established by the standard-star group PG 1633+099 (Landolt 1992). Color-color diagrams have been used to determine transformation equations from Gunn *r* and *i* to Johnson *R* and *I*. Reduction has been performed with IRAF (ver. 2.11.3a);[3] PSF photometry was achieved with IRAF/DAOPHOT. Limiting magnitudes are $B = 22.4$, $V = 23.0$, $R = 21.4$, and $I = 19.3$; the completeness limits have been estimated to be $B = 18.0$, $V = 17.5$, $R = 17.0$, and $I = 16.0$. The number of stars with photometry ranges from 547 stars in *B* to about 2000 in *i*. The major results for 46 OB stars are summarized in Table 1.

*JHKs* imaging was carried out in service mode in 2002 September with ISAAC (Moorwood et al. 1998) at the Very Large Telescope (VLT) (UT1). The pixel resolution was 0.148″; the effective spatial resolution was 0.6″ (FWHM). In order to cover the cluster area we observed a mosaic of 11 frames. At each position and in each filter 12 object and 12 sky frames were taken with the `ISAACLW_img_obs_AutoJitterOffset` template. This template allows the observer to obtain sky images in a circle around the initial telescope position and to jitter at each position; sky-throw (i.e., the radius at which sky frames were taken) and jitter-box width

[3] The Image Reduction and Analysis Facility is distributed by the National Optical Astronomy Observatory, which is operated by the Association of Universities for Research in Astronomy (AURA), Inc., under cooperative agreement with the National Science Foundation.

TABLE 1
High-Mass Stars in M17

| Name | R.A. (J2000.0) | Decl. (J2000.0) | Spectral Type: Optical | Spectral Type: $K$ Band | Spectral Type: $J$ Band | $V$ (mag) | $K$ (mag) | $A_V$ (mag) | DM |
|---|---|---|---|---|---|---|---|---|---|
| H997 | 18 20 14.2 | −16 14 00 | B1 V | | | 15.3 | 10.7[a] | 7.1 | 11.5 |
| H1520 | 18 20 17.5 | −16 08 19 | B2 V | | | 18.1 | 10.3 | 9.2 | 11.3 |
| CEN 35 | 18 20 21.5 | −16 09 39 | O9.5 V | O9.5 Ve | B | 17.1 | 10.1 | 9.5 | 11.7 |
| CEN 92 | 18 20 21.6 | −16 11 18 | B2 V | | | 20.1 | 8.8 | 13.4[b] | 9.1 |
| CEN 13 | 18 20 22.2 | −16 10 21 | B3 V | | | 12.4 | 10.7 | 3.4 | 10.5 |
| H3957 | 18 20 22.5 | −16 09 46 | B3 V | | | 21.6 | 11.4 | 12.3[b] | 10.9 |
| CEN 16 | 18 20 22.7 | −16 08 34 | 09 V | O9 V | O9.5 I | 13.2 | 9.0 | 6.9 | 10.6 |
| CEN 75 | 18 20 22.8 | −16 08 15 | B2 V | | | 18.1 | 11.8 | 8.6 | 11.9 |
| CEN 78 | 18 20 24.0 | −16 10 04 | B3 V | | | 17.9 | 11.1 | 8.5[b] | 10.9 |
| CEN 31 | 18 20 24.4 | −16 08 44 | O9.5 V | O9.5 V | O9.5 V | 15.5 | 9.2[a] | 7.1 | 12.6 |
| IRS 5 | 18 20 24.7 | −16 11 40 | | O6 V | | | 9.2 | 24.0[b] | 11.1 |
| M17−UC1 | 18 20 24.9 | −16 11 35 | B0 V | | | | 13.1 | | |
| CEN 49 | 18 20 25.3 | −16 10 19 | B2 V | | | 16.6 | 9.5 | 7.0 | 11.9 |
| CEN 36 | 18 20 25.3 | −16 09 40 | | O9.5 V | O | 17.7 | 10.5 | 9.8 | 12.1 |
| CEN 18 | 18 20 25.9 | −16 08 32 | O6 V | | | 13.7 | 7.8[a] | 8.5 | 10.1 |
| CEN 26 | 18 20 26.1 | −16 11 05 | B3 V | B3 V | B | 15.3 | 10.3 | 6.3 | 10.6 |
| CEN 48 | 18 20 26.3 | −16 10 16 | B3 V | B3 V | O9.5 V | 15.1 | 10.7 | 6.3 | 10.2 |
| CEN 52 | 18 20 26.6 | −16 10 23 | B0 V | | | 16.7 | 11.4 | 7.5 | 13.2 |
| CEN 51 | 18 20 26.6 | −16 10 03 | B3 V | | B | 17.2 | 9.5 | 8.1 | 10.6 |
| H6500 | 18 20 26.7 | −16 07 09 | B2 V | | | 17.5 | 8.6[a] | 10.4 | 9.6 |
| B240 | 18 20 26.8 | −16 07 49 | B0 V | O9.5 V | | 18.2 | 10.7 | 9.9 | 12.3 |
| CEN 23 | 18 20 27.3 | −16 10 25 | | B3 V | B | 14.0 | 12.2 | 3.3 | 12.3 |
| OI 345 | 18 20 27.4 | −16 13 32 | O6: V[c] | | | 11.3 | 7.4 | 4.3 | 11.9 |
| CEN 46 | 18 20 27.8 | −16 11 02 | | O9 V | Late O I | 17.1 | 9.4[a] | 10.2 | 11.3 |
| CEN 47 | 18 20 27.9 | −16 11 09 | | O9.5 V | B | 16.3 | 10.6 | 8.1 | 12.3 |
| CEN 65 | 18 20 28.0 | −16 10 59 | | O9 V | O: | 16.2 | 10.1 | 8.1 | 12.4 |
| IRS 15 | 18 20 28.7 | −16 12 12 | B0.5 V | B0 V | B1 V | 16.1 | 9.8 | 7.4 | 12.4 |
| CEN 30 | 18 20 28.7 | −16 09 26 | O9 V | O9 V | B1 V | 16.7 | 10.7 | 8.9 | 12.2 |
| CEN 55 | 18 20 29.1 | −16 10 54 | B0 Ve | | early B I | 17.3 | 10.4 | 9.8 | 11.5 |
| CEN 42 | 18 20 29.2 | −16 11 11 | B2 V | | | 15.7 | 10.3 | 7.8 | 10.4 |
| CEN 59 | 18 20 29.4 | −16 10 56 | | B0 V | B | 17.0 | 10.0 | 10.1 | 10.9 |
| CEN 27 | 18 20 29.8 | −16 11 37 | O9 V | O9 V | B | 17.2 | 9.6 | 10.2 | 11.3 |
| CEN 1b | 18 20 29.8 | −16 10 46 | O4 V | O4 V | O4 V | 14.9 | 6.9 | 13.5 | 10.7 |
| CEN 1a | 18 20 29.9 | −16 10 44 | O4 V | O4 V | O4 V | 13.5 | 6.9 | 10.2 | 11.3 |
| CEN 61 | 18 20 30.2 | −16 10 35 | O9 V | O? | | 16.9 | 9.0[a] | 10.5 | 10.7 |
| CEN 37 | 18 20 30.4 | −16 10 53 | O6 V | O6 V | O6 V | 19.3 | 7.6[a] | 14.1[b] | 10.2 |
| CEN 25 | 18 20 30.9 | −16 10 08 | O7 V | O7 V | O9 I | 14.9 | 8.8[a] | 8.5 | 11.1 |
| CEN 28 | 18 20 31.8 | −16 11 38 | B2 V | O9 V: | | 15.4 | 11.2 | 5.5 | 12.3 |
| B140 | 18 20 32.9 | −16 12 40 | | B3 V: | B | 12.1 | 10.8 | 2.0 | 11.6 |
| CEN 43 | 18 20 33.1 | −16 11 22 | O5 V | O4 V | O5 V | 17.8 | 8.1[a] | 10.1 | 12.9 |
| CEN 29 | 18 20 33.1 | −16 10 14 | O9 V | | | 17.3 | 10.4[a] | 9.5 | 12.1 |
| CEN 2 | 18 20 34.5 | −16 10 12 | O5 V[c] | | | 11.2 | 7.5[a] | 4.0 | 12.5 |
| H12556 | 18 20 35.2 | −16 08 43 | B3 V | | | 19.5 | 12.0 | 9.2[b] | 11.8 |
| CEN 3 | 18 20 35.4 | −16 10 49 | O9 V[c] | O9 V | Late O I | 9.9 | 7.7 | 3.8 | 10.4 |
| CEN 45 | 18 20 35.6 | −16 10 56 | B2 V | | | 12.9 | 10.7 | 3.7 | 11.6 |
| B58 | 18 20 37.9 | −16 07 32 | B0: V | | | 16.3 | 10.2 | 6.8 | 13.5 |

Notes.—Extinction and distance modulus have been obtained from optical data whenever available. Units of right ascension are hours, minutes, and seconds, and units of declination are degrees, arcminutes, and arcseconds. Designations: "CEN" (Chini et al. 1980), "H" this work, "B" (Hanson et al. 1997), "IRS" (Chini & Wargau 1998), "OI" (Ogura & Ishida 1976), "M17-UC1" (Felli et al. 1984).

[a] Photometry from 2MASS.

[b] $A_V$ from IR colors.

[c] Spectral type from literature.

were 600″ and 10″, respectively. The central position is R.A. = $18^h20^m25.5^s$, decl. = $-16°10'40''$ and the field size is $6.8' \times 8.8'$. About 95% of the stars have photometric errors below 0.1 mag for $J = 18.9$, $H = 18.3$, and $K = 17.2$. Standard photometric calibration has been achieved with the sources 9106, 9116, 9172, 9181, and 9185 from Persson et al. (1998). The total number of stars and the corresponding limiting magnitudes are $J =$ 4990 (20.9), $H =$ 10730 (20.4), $Ks =$ 18504 (20.1); estimates of the completeness limits yield $J = 18.0$, $H = 18.0$, and $Ks =$ 17.5. The data have been reduced and analyzed with standard procedures using IRAF and IRAF/DAOPHOT, respectively. Figure 1 shows a *JHK* mosaic of the area providing the so far deepest look into the young cluster.

$L'$-band data were obtained in service mode between 2004 May and September with ISAAC at a central wavelength of 3.78 $\mu$m and a bandwidth of 0.58 $\mu$m. The data have been taken with the

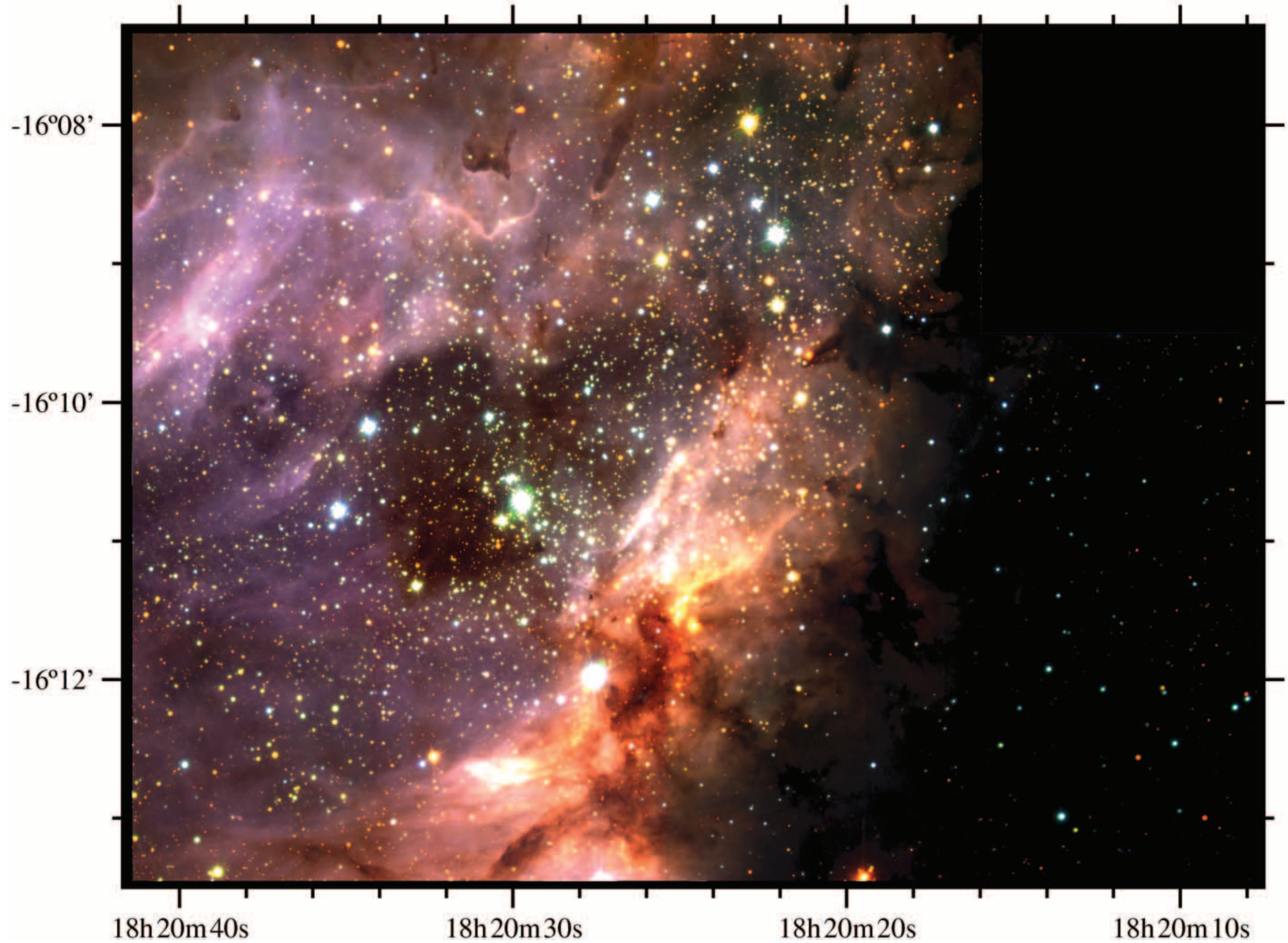


FIG. 1.—*J* (*blue*), *H* (*green*), and *K* (*red*) mosaic of the M17 cluster obtained with ISAAC at the VLT.

`ISAAC_img_obs_AutoChopNod` template. The pixel resolution was 0.07″; the effective spatial resolution was 0.4″ (FWHM). The cluster was covered by a grid of 29 positions around the central position R.A. = $18^h20^m29.8^s$; decl. = $-16°10'18''$, resulting in a field of view of $5.5' \times 5.6'$—slightly smaller than the *JHK* mosaic. The data have been reduced and analyzed with IRAF and IRAF/DAOPHOT. Due to the absence of photometric standards, calibration was accomplished by using 67 stars in M17 whose *L*-band magnitudes were published by Chini & Wargau (1998).

Our PSF photometry comprises ~3200 sources down to a limit of $L = 15.6$ mag. The detection rate for *L*-band sources decreases in the northern and the southern bar of M17. This is a consequence of the emission from extended hot interstellar dust and PAHs which enhances both the background and the confusion in those regions. Nevertheless, we can exclude false detections at *L* to a large extent: There are 46 sources that have been detected only in the *L*-band. These detections either belong to bright stars which are saturated at *JHK* or they are fainter companions of bright stars that were resolved by our *L*-band images but which could not be resolved at *JHK*. However, due to the lack of photometric data at shorter wavelengths, these sources are not contained in the results of this paper. In order to derive a completeness limit we have added artificial stars and checked for their recovery. At $L = 13$ we achieved a situation for which the detection rate was uniform over the entire field.

### 2.2. *Spectroscopy*

We performed optical low-dispersion long-slit and multiobject spectroscopy for a total of 403 stars. Their apparent brightness span a range from $I = 7.5$ to 18 mag, and our optical spectroscopy is almost complete within this magnitude range. Less than a dozen of sources are missing due to the automatic fiber positioning procedure. The stars are distributed homogeneously across the cluster field of Figure 1. The first data set was obtained in 2005 September with EMMI (Dekker et al. 1986) at the ESO NTT; the slit dimensions of the long-slit and the MOS were $1.5'' \times 8'$ and $1.0'' \times 8''$, respectively; grism 2 provides a wavelength coverage of 3800–9200 Å, with an average spectral resolution of $R \sim 570$. We observed five different slit positions and two masks providing us with 80 spectra. Standards from Silva & Cornell (1992) have been used to determine stellar temperatures and luminosity classes. Ultimately, 74 sources could be classified with sufficient signal-to-noise ratio. Data reduction and analysis was carried out with standard IRAF procedures.

Optical fiber spectroscopy has been carried out in 2006 April and May with FLAMES using GIRAFFE/MEDUSA (Pasquini et al. 2002) at the ESO VLT; the observations were carried out in low-resolution mode L881.7 providing a spectral resolution of $R \sim 6500$. We observed four different fiber allocations each for 1 hr with approximately 80 objects and 25 sky fibers, resulting in a total of 323 observed individual sources. The pipeline processed images were further analyzed with IRAF. Spectral classification was accomplished with standards from Bagnulo et al. (2003). The results concerning spectral type are summarized in Table 1 for the early-type stars and in Figure 6 for 318 potential cluster members.

We took $J$- and $K$-band spectra for 33 and 201 stars, respectively. The data was taken in the summer of 2004, 2005, and 2006 with ISAAC at UT1. $K$-band spectroscopy was performed with a $0.3'' \times 120''$ slit in short-wavelength low-resolution mode, yielding a spectral resolution of 1500. $J$-band spectra were obtained with a $0.6'' \times 120''$ slit in short-wavelength medium-resolution mode, resulting in a spectral resolution of 5700. We have used the `ISAACSW_spec_obs_AutoNodOnSlit` template, nodding the telescope between two positions (A and B) along the slit. At each position 2 or 4 images have been obtained depending on the brightness of the objects. If the nod throw is not too large, subtraction of AB pairs reduces the sky background fairly well. Unlike the sky background the nebular background is inhomogeneous and cannot be subtracted in this way. Therefore, we have fitted the background during the extraction for each object individually and if necessary several times to optimize the nebular background subtraction. Wavelength calibrations were made with arc spectra and OH sky lines (Rousselot et al. 2000) in the $K$ and $J$ band, respectively. The data has been reduced and analyzed with standard IRAF procedures.

The selection and spatial distribution of the sources across the field in Figure 1 was fairly arbitrary. We centered one or two of the brighter sources on the $120''$ slit, while on average two to three additional sources happened to be covered by the same slit position. In this way, more than half of the stars entered our IR-sample by pure chance. The IR-sources span an apparent brightness range from $I \sim 8$–20 mag for both the $J$- and $K$-band sources. In summary, both groups (optical+IR) provide a representative magnitude limited sample down to about $I \approx 18$ mag with a uniform field coverage.

## 3. THE EXTINCTION TOWARD M17

The total extinction for stars in M17 is composed of a foreground fraction described by a ratio of total-to-selective extinction of $R = 3.1$ plus a local fraction of dust inside M17 with a possible higher $R$-value. A further grain population might exist in the case of circumstellar disks and shells. Obviously, the separation of these contributions is mandatory for a proper distance determination but extremely difficult. Early low-resolution measurements (e.g., Dickel 1968; Ishida & Kawajiri 1968) yielded an east-west gradient of the extinction, starting at $A_V = 1$ mag toward the H II region and reaching a maximum of $A_V = 7$ mag toward the central absorbing dust filament in front of the cluster. Glushkov et al. (2005) presented the most detailed measurements and derived $A_V$ values for the eastern, optically bright part of the nebula of 2–6 mag. This minimum extinction of $A_V \sim 1$–2 mag located in front of the H II region is in good agreement with Galactic models that predict values of $A_V \sim 2.7$ mag at a distance of 2 kpc in the direction of M17 (Bahcall & Soneira 1980). As discussed later, typical extinction values for cluster members are above $A_V = 2$ mag.

To investigate deviations from the general extinction law, characterized by $R = 3.1$, we compare the distance modulus $V - M_V$ with the color excess $E_{B-V}$ (Fig. 2). This method of "variable extinction" has been introduced by Johnson & Hiltner (1956) and is sensitive to both the $R$-value and the distance. It can be applied whenever stars in a stellar aggregate suffer from a large range of extinctions. $V$ is the apparent, $M_V$ the absolute visual brightness as obtained from our optical spectroscopy (see Table 1). To exclude

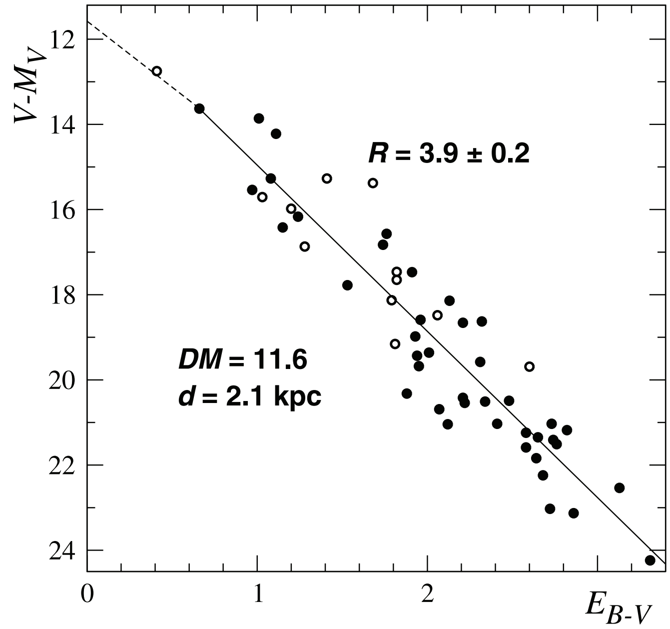


FIG. 2.—Distance modulus vs. color excess for 53 O- and B-type stars in M17 with $A_V > 2$ mag (*filled circles*) B3 and earlier, (*open circles*) later B3. The fit to the data (*solid line*) yields $R = 3.9 \pm 0.2$. The dashed line corresponds to the contribution of foreground extinction ($A_V = 2$ mag) with $R = 3.1$.

contamination from foreground stars, only spectroscopically classified early-type stars with $A_V > 2$ mag were used; simultaneously, this selection omits low-mass PMS objects from the sample. The slope of the linear least-squares fit corresponds to the ratio of total to selective extinction and yields $R = 3.9 \pm 0.2$. This result is a further independent support for a higher than normal $R$-value in M17 and is based on a unprecedented number of spectroscopically classified early-type stars in the region.

## 4. THE DISTANCE TO M17

We use three independent methods to derive the distance for M17. Most data used for these estimates are summarized in Table 1 and are based on those early-type stars; their relatively high extinction ($A_V > 3$ mag) and their early spectral type suggest that they are cluster members.

### 4.1. *Method of "Variable Extinction"*

The principles of this method have been outlined in § 3. In the case of M17 there is the complication in that the reddening law is different in the foreground and in the H II region. As a consequence, the transition between normal and special reddening influences the extrapolation to $E_{B-V} = 0$ for deriving the distance modulus. Adopting the results from the previous section concerning the foreground extinction of ~2 mag we extrapolate the dashed line in Figure 2 (corresponding to a reddening slope of $R = 3.1$) which starts at $E_{B-V} = 0.65$ to 0. This yields a distance modulus of 11.6 mag corresponding to 2.1 kpc. A different contribution of foreground extinction, say of 3 or only 1 mag, would change this value by ±0.2 kpc, respectively.

### 4.2. *Individual Distance Moduli*

Next we average the individual distance moduli (DM) of 45 stars from Table 1 by using a foreground extinction $A_V = 2$ mag and a reddening law with $R = 3.9$ for $A_V > 2$ mag. The mean distance modulus is DM $= 11.6 \pm 0.1$ equivalent to a distance $d = 2.1 \pm 0.1$ kpc.

Hanson et al. (1997) derived a rather low mean distance modulus of $10.5 \pm 0.4$ based on five O-type stars. It seems, however, that multiplicity has contaminated this estimate severely: CEN 3 (≡B98), the star with the lowest distance modulus in sample of Hanson et al. (1997) has been treated as a single object by these authors. Our high-resolution *JHK* imaging shows that within the $3.6''$ aperture used for the photometry quoted by Hanson et al. there are three stars: CEN 3 itself is barely resolved into two (almost) equally bright components at *K*; a third, very red star $2.5''$ to the southeast is 0.7 mag fainter than (the double) CEN 3. This explains both the low distance modulus and the low *R*-value obtained by Hanson et al. for CEN 3. Another example is CEN 18 (≡B260), the star with the second lowest distance modulus in sample of Hanson et al. (1997). Our optical spectra show that it is a spectroscopic binary with equally bright double Paschen lines, suggesting that the combined *K*-band brightness of the two components—as used by Hanson et al.—severely underestimates the distance. CEN 37 (≡B174) is also a barely resolved binary in our IR images.

### 4.3. *Luminosity Distance*

Compared to the study by Hanson et al. (1997) Table 1 contains 32 new spectroscopically classified high-mass stars that contribute to the ionization of M17; the multiple O stars and the hypercompact H II region M17-UC1 have been omitted from this statistics. Obviously, the considerably increased number of early-type stars requires a revision of the luminosity distance as presented by Povich et al. (2007). These authors obtain a total luminosity of $L_{\rm SED} = 2.4 \pm 0.3 \times 10^6\ L_\odot$ from the spectral energy distribution of the nebula by adopting a distance of 1.6 kpc. Using the conversion by Crowther (2005) the luminosity provided by the OB stars in Table 1 is $L_{\rm OB} = 3.8 \times 10^6\ L_\odot$ at a distance of 2.1 kpc. Taking into account the multiplicity of CEN 1 a and b (see § 5), CEN 3, 18, and 37, and assuming for simplicity that all of them have an equal-mass companion, the total stellar luminosity would increase to even $5.2 \times 10^6\ L_\odot$. Scaling the distance in such a way that $L_{\rm SED}$ equals $L_{\rm OB}$, we obtain a minimum distance of $d_{\rm min} = 2.0$ kpc (2.35 kpc including the four binary O stars).

In summary, all new methods exclude earlier distance estimates significantly below 2 kpc and argue in favor of a distance of $d = 2.1$ kpc. This value is in accordance with the kinematic results as well as with the early photometric estimate by CEN80 and is used throughout the paper.

## 5. GENERAL CLUSTER PROPERTIES

The cluster area investigated at *JHK* is displayed in Figure 1. Before discussing some global properties of the cluster we investigate the questions of infrared excess and cluster membership in more detail.

### 5.1. *IR Excess Objects*

Young stars are expected to be accompanied by circumstellar disks which can be detected through the emission of heated dust. Ground-based observations allow the search for such disks by comparing the total IR flux with that expected from the stellar photosphere. It has been shown that IR excess emission from circumstellar disks are much more easily detectable at *L* than at *K* (Strom et al. 1989; Lada et al. 2000).

Although the definition of an object with IR excess (IRE) seems evident, in practical terms it depends on a variety of assumptions, particularly when the excess emission is derived from NIR color-color diagrams. Here the adopted intrinsic colors are just as important as the slope of the reddening path. The combination of both spans the width of a region in which stars are regarded as excess free. MIR observations suffer from this problem to a much lesser extent.

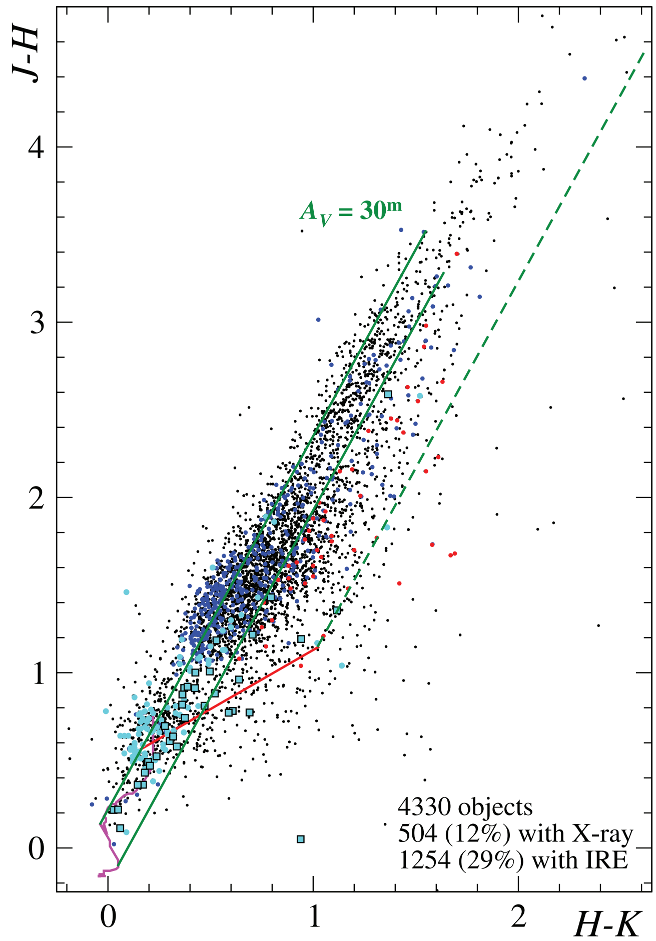


Fig. 3.—*JHK* diagram of 4330 stars toward M17. The solid magenta curve denotes the locus of unreddened main-sequence stars (Ducati et al. 2001); the red line corresponds to the locus of T Tauri stars (Meyer et al. 1997). Reddening vectors with a length of $A_V = 30$ mag are drawn. Cyan symbols refer to spectroscopically classified stars (*open squares*: high-mass stars from Table 1; *filled circles*: intermediate- to low-mass stars). Blue symbols characterize stars with X-ray emission. Red dots are stars with *K* excess that does not show up as *L* excess. The diagram includes only data points with photometric errors less than 0.1 mag at each wave band. One extremely red source with $H-K = 3.6$ is not displayed (see text).

Figure 3 shows the most common IR color-color diagram composed of *JHK* data of 4330 stars toward M17; the photometric errors are less than 0.1 mag at each wave band. The color excess ratio $E(J-H)/E(H-K)$ may change as an object gets more and more reddened due to the shifts of effective wavelengths of the filters (Jones & Hyland 1980; Nagata et al. 1993; Fitzpatrick 1999). This can result in deviations from the straight reddening line in the color-color diagram, and the deviations depend on individual photometric systems. The slope of the reddening vector in Figure 3 has been determined by fitting the locus of reddened main-sequence stars, similar to the method described by (Kenyon et al. 1998). This yields a value of $E(J-H)/E(H-K) = 2.06 \pm 0.01$ which is compatible with the value expected from the relations given by Cardelli et al. (1989). Within the photometric errors and the uncertainties introduced by color transformations (Naoi et al. 2006) as well as by the presence of PMS stars there is no indication for a curvature of the ratio $E(J-H)/E(H-K)$. Thus, using a straight relation $E(J-H)/E(H-K) = 2.06$, we derive

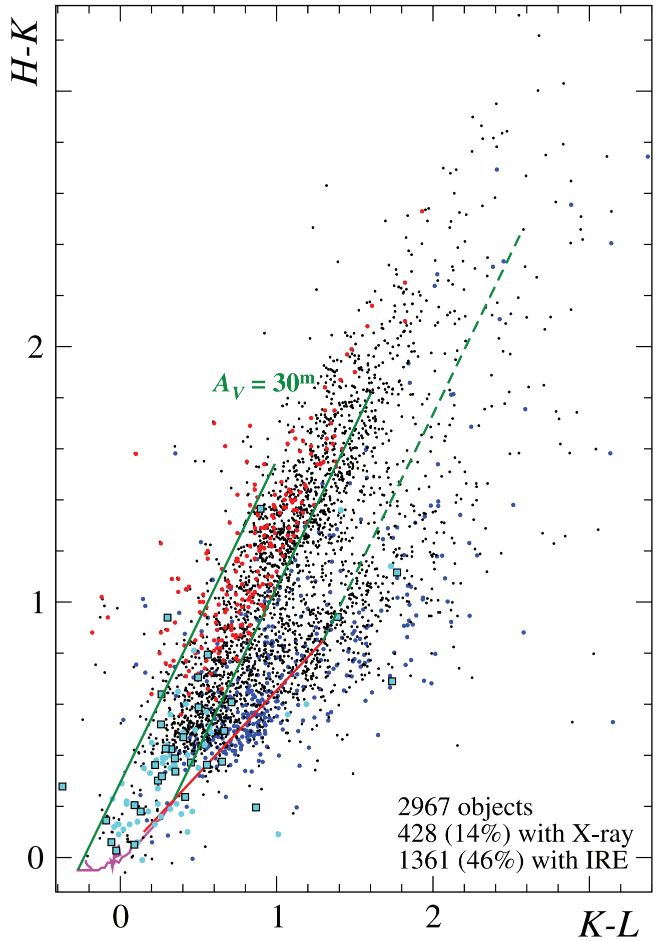


FIG. 4.—*HKL* diagram of 2967 stars toward M17. Lines, symbols, and errors are as in Fig. 3. Reddening vectors with a slope of $E(H-K)/E(K-L) = 1.2$ and a length of $A_V = 30$ mag are drawn.

that 1254 objects (29%) are located formally in the excess region of Figure 3; these sources are referred to as "stars with *K* excess."

Figure 4 shows the *HKL* color-color diagram which contains 2967 stars toward M17 with photometric errors less than 0.1 mag at each wave band. Fitting the locus of reddened main-sequence objects yields a value of $E(H-K)/E(K-L) = 1.19 \pm 0.01$ which is again compatible with an extinction law described by Cardelli et al. (1989). In this diagram there are 1361 objects (46%) located formally within the excess region; in the following these sources are referred to as "stars with *L* excess."

As is to be expected, the fraction of IRE objects increases, from 29% to 46%, when going from the *JHK* diagram (Fig. 3) to the *HKL* diagram (Fig. 4). These numbers would increase to 37% and 57%, respectively, if the intrinsic colors given by Bessel & Brett (1988) were adopted instead of those published by Ducati et al. (2001). Comparing the results from the two diagrams (*JHK* vs. *HKL*) for stars that have measurements at *JHKL*, there are 223 stars with *K* excess that do not show *L* excess; these are marked as red dots in Figures 3 and 4. Vice versa, there are 621 stars with *L* excess but without *K* excess. While the latter result is within expectations, the reason for sources displaying only *K* excess is less clear. One reason is certainly due to the formal selection of sources located left of the reddening path in Figure 3. This is a general procedure used when determining IRE from color-color diagrams (Lada et al. 2000; Haisch et al. 2001b), but it neglects the fact that observational errors may shift normal stars just beyond the reddening path into the excess region. Vice versa, stars with true IRE may be shifted into the normally reddened region by the same effect, probably keeping the total number of IRE objects constant. Therefore, introducing a minimum distance from the reddening path beyond which a source is regarded as a true IRE object will underestimate the total number of IRE objects. Variability might be another effect because the *L*-band data were obtained several months after the *JHK* data. In fact, 39 stars with *K* excess in Figure 3 lie in the "forbidden" region above the upper reddening path in Figure 4 which suggests that these stars are variable. Despite the above caveats, henceforth we use the term IRE for stars which have a formal excess either at *K* or at *L*.

### 5.2. *Cluster Membership*

In the absence of proper-motion studies, we have to use indirect arguments to exclude contamination by unrelated field stars. One argument comes from the X-ray emission of stars toward M17. As discussed extensively by Broos et al. (2007), there are about 20 extragalactic sources and an equal number of galactic foreground stars to be expected among the ACIS sources within a field of $17' \times 17'$. If we scale these numbers to the field size of our NIR observations we expect only six sources with X-ray emission that are not related to M17. Given that foreground stars can probably be excluded by their low visual extinction ($A_V <$ 1–2 mag), there remain about three possible extragalactic X-ray sources in our sample; the latter, however, are unlikely to be detectable in the IR. We therefore assume in the following that X-ray emission is a reliable indicator for cluster membership.

There are altogether 18,883 stars detected at *K*; obviously, all 606 ACIS sources contained in the cluster field of Figure 1 have IR counterparts. The matching between ACIS and NIR was performed by using positional coincidence criteria. Because our IR data and the ACIS field were both aligned to 2MASS there were no reference frame offsets between the two data sets. Using the software package ALADIN we looked for IR sources within $1''$ of the X-ray source. In more than 50% of the cases the `cross match` routine found only a single source within the search field, making the decision unique. In crowded locations there were multiple IR sources satisfying the match condition for a specific ACIS source. In such situations we chose the closest IR match of the group. Very few (<3%) constellations showed two IR sources at the same close distance from the ACIS source. In these cases we took the brighter IR source as the most likely counterpart. This selection is justified by the fact that apart from 23 stars, all X-ray sources are brighter than $K = 16$; in contrast, the questionable candidates were always fainter than $K = 18$ and could thus be excluded.

Infrared excess which is most likely due to circumstellar dust is another argument for the youth of the corresponding objects and their relation to the star formation in M17. Therefore, we regard all stars with IRE at *K* and/or *L* as cluster members.

Among the 4330 stars in Figure 3 there are 504 (12%) X-ray sources and 1254 (29%) stars with IRE. A decision on the membership of "normal" stars can only be attempted on the basis of their reddening. The *JHK* diagram shows two concentrations of sources with a gap at about $0.8 < J-H < 1.1$. If this gap were purely due to extinction it would correspond to about $7 < A_V <$ 10 for early-type stars. Jiang et al. (2002) report a similar gap in their *JHK* diagram and interpret the two groups of objects as "*unreddened (foreground) stars and reddened (cluster member and background) stars*," respectively. In order to examine the membership of these two concentrations of stars, we consider several arguments on extinction, IRE, and X-ray emission.

There is little doubt that most of the heavily reddened stars above the gap in Figure 3 belong to the embedded cluster, as

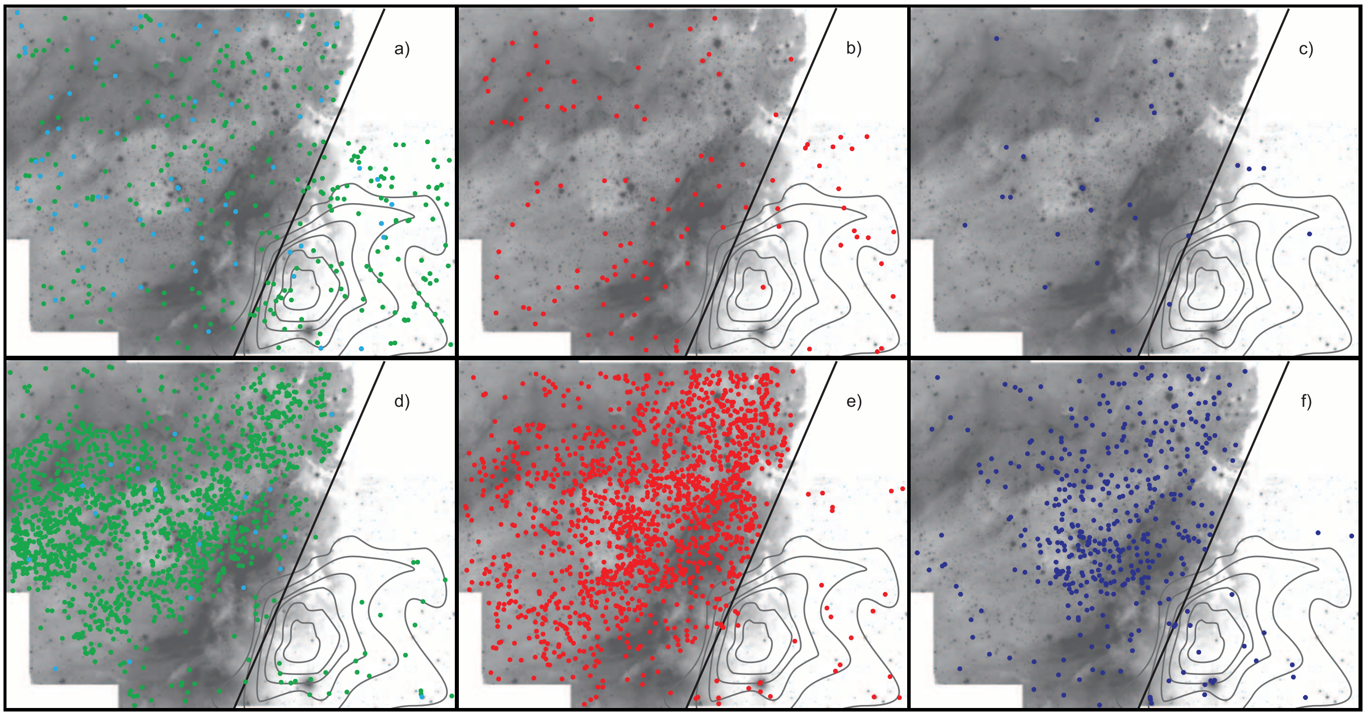


Fig. 5.—Spatial distribution of stars toward M17 grouped according to their position in Fig. 3; the gray-scale image in the background is the $K$-band mosaic. *Top row*: 497 stars from the less reddened group ($J - H < 0.8$) which have been claimed foreground by Jiang et al. (2002). (*a*) 270 normal sources (*green*); 82 spectroscopically classified members (*cyan*). (*b*) 118 IR excess sources (*red*); (*c*) 27 sources with X-ray emission (*blue*). *Bottom row*: Stars from the heavily reddened group ($J - H > 1.1$), with the same notation as above. The straight line crudely separates the nebular region from the southwestern molecular cloud, which is denoted by the gray $C^{18}O$ contours adapted from Wilson et al. (2003).

witnessed by numerous IRE and X-ray sources among this sample. Likewise, there are many sources showing the 2.3 $\mu$m CO band in emission or absorption that share, e.g., the same range of visual extinction. In fact, the "reddest" source in the *JHK* sample, with $H - K = 3.6$ (not shown in Fig. 3), is not a background star: it is an X-ray source, has IRE, and shows the CO bandhead feature in emission (Hoffmeister et al. 2006). In addition, Figure 4 suggests that a large fraction of stars with $A_V > 30$ mag—i.e., the most promising candidates for stars lying behind M17—have IRE and thus are probably cluster members. We therefore conclude that the opaque molecular cloud behind the H ii region acts as a shield between background stars and cluster members and—as a consequence—most, if not all, stars from the heavily reddened group with $J - H > 1.1$ are cluster members.

The group of 497 less-reddened objects below the gap, i.e., those with $J - H < 0.8$, contains 19 (4%) spectroscopically classified OB stars, 27 (5%) objects with X-ray emission, and 118 (24%) stars with IRE. Those stars are certainly cluster members. In addition, we have spectroscopy for 107 intermediate- and low-mass stars (later B3) within this less-reddened group; 63 (13%) of them have $A_V > 2$ mag. From the results in § 3 it is very likely that these stars also belong to M17 on the basis of their visual extinction. In summary, we can classify 227 (46%) stars in the less-reddened group as secure or very probable cluster members; further sources for which spectroscopy is still missing may turn out as additional members. Thus, the interpretation by Jiang et al. (2002) that this entire group consists of unreddened (and thus unrelated) foreground stars must be discarded.

Figure 5 compares the spatial distribution of the two groups; a crude dividing line has been drawn to separate the nebular region from the southwestern molecular cloud. Those 352 "normal" stars of the less reddened group that display neither IRE nor X-ray emission (Fig. 5*a*) show a fairly homogeneous distribution across the entire field (*green dots*). However, the 82 spectroscopically classified members (*cyan dots*) among this sample are located mainly toward the H ii region. Likewise, Figures 5*b* and 5*c* corroborate the finding that 145 stars with IRE and/or X-ray emission, i.e., cluster members, prefer locations toward the H ii region, i.e., left of the line. Interestingly, 1539 normal members of the heavily reddened group are also located in the area of the nebula (Fig. 5*d*), like the most heavily reddened sources with IR and X-ray emission (Figs. 5*e* and 5*f*), thus corroborating their membership. Only few objects are located toward the southwestern molecular cloud (hereafter "cloud B"), suggesting that the star formation (SF) has not yet proceeded much beyond the indicated line.

Table 2 summarizes the statistics from the sources in the *JHK* diagram (Fig. 3) and from their spatial distribution (Fig. 5). For that purpose the sample has been divided into "low" and "high" reddening sources according to $J - H < 0.8$ and $J - H > 1.1$; furthermore, a crude division between the "H ii region" and the southwestern molecular "cloud B" has been made according to the position of the stars right or left of the line along the interface in the southwest (Fig. 5). The nonnegligible influence of the adopted intrinsic colors is shown by using values from Ducati et al. (2001) and Bessel & Brett (1988); the latter reference leads to an increase of IRE sources of up to 12%.

Among the 2967 stars in the *HKL* color-color diagram (Fig. 4) there are 428 (14%) X-ray sources and 1361 (46%) objects with IRE. The above-mentioned gap in the *JHK* color-color diagram (Fig. 3), which should occur at about $H - K \sim 0.3$, seems to exist but is hardly visible due to the low number of stars with bluer colors. The gap also vanishes in the *JHK* diagram when plotting only sources with detections at $L$.

Both color-color diagrams show that cluster members of M17 which were identified on the basis of their X-ray and IRE emission

TABLE 2

Statistics of Sources from the *JHK* Diagram

| Normal | IRE | X-Ray | Normal | IRE | X-Ray | Intrinsic Colors |
|---|---|---|---|---|---|---|
| H ii Region ($N = 3620$) | | | | | | |
| $J - H < 0.8$ ($N = 347$) | | | $J - H > 1.1$ ($N = 3280$) | | | |
| 230 (68%) | 95 (28%) | 22 (6%) | 1539 (47%) | 1532 (47%) | 396 (12%) | Ducati et al. (2001) |
| 211 (62%) | 116 (34%) | 22 (6%) | 1225 (37%) | 1972 (59%) | 396 (12%) | Bessel & Brett (1988) |
| Cloud B ($N = 226$) | | | | | | |
| $J - H < 0.8$ ($N = 150$) | | | $J - H > 1.1$ ($N = 76$) | | | |
| 122 (81%) | 23 (15%) | 5 (3%) | 43 (57%) | 33 (43%) | 0 (0%) | Ducati et al. (2001) |
| 141 (76%) | 31 (21%) | 5 (3%) | 36 (47%) | 40 (53%) | 0 (0%) | Bessel & Brett (1988) |

suffer from extinction over a large range ($2 < A_V < 50$). We therefore suggest that most of the remaining objects (~2000) within the heavily reddened group are likely cluster members too; because not all of them were measured at all four wave bands, they do not show up simultaneously in all color-color (Figs. 3 and 4) and color-magnitude diagrams (e.g., Fig. 8). Broos et al. (2007) extrapolate 8000–10,000 cluster members on the basis of the X-ray luminosity function. This estimate is consistent with the current study, given the large number of $K$-band sources that could not be observed at $J$ and $H$. Within the less-reddened group there are 285 sources left that have no spectroscopy and neither X-ray nor IRE emission; they are potential foreground candidates. Future X-ray observations of higher sensitivity or IR variability studies and spectroscopy might reduce this number even more. One must therefore conclude that the statistics of this rich cluster are not severely contaminated by unrelated field stars; the numbers above suggest a frequency of $\leq 3\%$.

### 5.3. *The Optical HR Diagram*

Figure 6 shows an optical HR diagram that contains 318 stars which have been classified by their optical spectra. The extinction-corrected visual brightness was derived by splitting the observed $E_{B-V}$ into a foreground and a local fraction, as explained above; the intrinsic color $(B-V)_0$ is taken from the spectral type, using the conversion by Schmidt-Kaler (1982). To avoid contamination by unrelated foreground stars, only objects with $A_V > 2$ mag have been included. Among the early-type stars in Figure 6 there are 28 X-ray emitters (Broos et al. 2007), while 16 of them display IRE probably originating from remnant circumstellar material. A zero-age main-sequence (ZAMS) for 2.1 kpc is compatible with the data, although the steepness of the curve would allow for a much broader range of—preferentially larger—distances.

There are four stars in Figure 6 which are located above the position of an O3 star. The fact that these stars are brighter than what is expected from their spectral type (see Table 1) is likely due to their multiplicity. Two of them are the components of CEN 1, the major ionizing sources in the field. The northeastern component is located at R.A. $= 18^{\rm h}20^{\rm m}29.89^{\rm s}$ and decl. $= -16°10'44.5''$ (hereafter referred to as CEN 1a) and has $V_0 = 4.8$ mag. It shows double Paschen lines in the optical and IR (Fig. 7). The southwestern component (hereafter referred to as CEN 1b), also with $V_0 = 4.8$ mag, is located at R.A. $= 18^{\rm h}20^{\rm m}29.81^{\rm s}$ and decl. $= -16°10'45.7''18$. Its $J$-band spectrum also shows a double Pa $\delta$ line. CEN 18 ($V_0 = 5.2$ mag) is a spectroscopic binary with equally bright double Pa 11 lines. A reduction by 0.75 mag, as appropriate for a binary with identical components, would shift CEN 18 down into the early O-type region. Finally, there is CEN 37 with $V_0 = 5.3$ which is also a probable binary.

### 5.4. *High-Mass Stars and Energy Balance*

So far, two studies were particularly devoted to the high-mass members of the M17 cluster. Hanson et al. (1997) presented a multiwavelengths spectroscopic survey of 13 known OB star candidates in the cluster and corroborated or improved their spectral type designations. However, no further massive candidates could be added compared to the early photometric study by CEN80. Nielbock et al. (2001) concentrated on the circumstellar environment of some of these massive stars presenting 10 and 20 $\mu$m imaging of the area. The SEDs and the morphology of the MIR emission strongly suggested that some massive stars are surrounded by circumstellar dust.

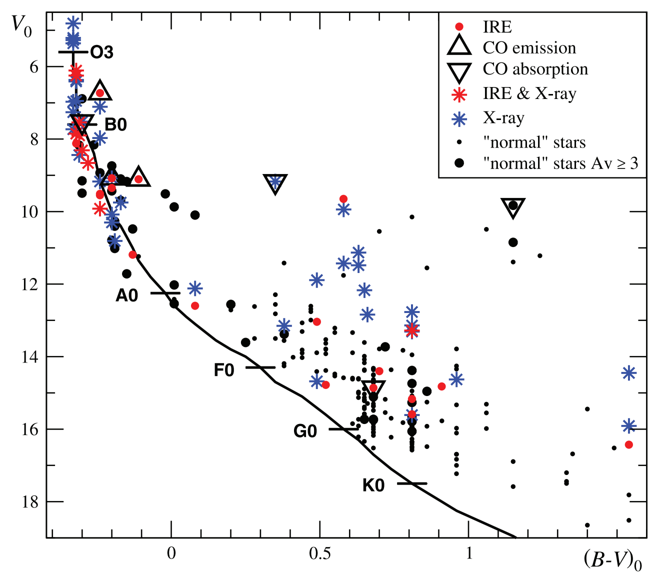


Fig. 6.—Dereddened color-magnitude diagram for 318 spectroscopically classified stars with $A_V > 2$ mag. Blue asterisks denote X-ray emission and red symbols mean stars with infrared excess (IRE); see § 5.1. Black dots are normal stars without X-ray emission or IRE; large symbols correspond to $A_V \geq 3$ (most likely cluster members); small symbols refer to $A_V > 2$ (potential members). Triangles show sources with the 2.3 $\mu$m CO band-head feature (Hoffmeister et al. 2006). The curve is a ZAMS of 2.1 kpc which is compatible with all data points, taking into account the photometric errors of <0.1 mag at each wave band. Beyond $(B-V)_0 = 0.0$ the first spectroscopically classified PMS stars in M17 become visible.

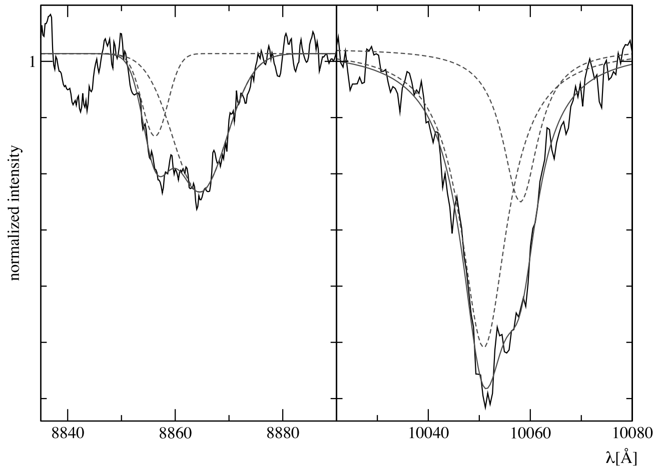


FIG. 7.—Spectroscopy of CEN 1 a. *Left*: Pa 11 at $\lambda_0 = 8860$ Å. The line profile has been fitted by two components (dashed curves) with a velocity difference of 280 km $s^{-1}$. The resulting line profile is shown by the solid curve. *Right*: Pa $\delta$ at $\lambda_0 = 10049$ Å, with the same notation as above. The velocity difference here is 215 km $s^{-1}$. The location of CEN 1 a above the location of an O3 star in Fig. 6 suggests that both components are of similar spectral type. [*See the electronic edition of the Journal for a color version of this figure.*]

The unbiased spectroscopic study of the present work led to the detection of 33 additional early-type stars. Table 1 summarizes the latest results on massive stars in M17. The major ionization of M17 is provided by two O4 V stars in the cluster center. Kleinmann (1973) classified this "*anonymous star*" as "*double O or early B*." CEN80 obtained a double O4 type (CEN 1) but realized that one of the components suffers from larger extinction. Spatially unresolved spectroscopy for both components (Hanson et al. 1997) yielded a combined spectral type of O5 V (optical) and kO3–O4 (*K*-band). We could obtain both resolved multicolor photometry and spectroscopy of the two components of CEN 1 which are separated by 1.8″. On the basis of our spectroscopy both components are classified as O4. As mentioned above, both components are also spectroscopic binaries which makes CEN 1 into a Trapezium-like system. The photometry indicates that CEN 1a and 1b are reddened by $A_V = 10$ and 13 mag, respectively. If CEN 1 is a physical binary system, this large difference can only be explained by a highly clumped interstellar medium along the line of sight. Another large difference in extinction has been found for the companion of CEN 3 on a scale of 2.5″. As mentioned in § 4 some of the other O-type stars also appear as spectroscopic binaries in our optical and NIR spectra, thus increasing the number of high-mass stars even more.

Despite the increase of known high-mass stars in the present work (46 vs. 13) the Lyman continuum flux indicates that further exciting stars must be embedded in the cluster. The number of Lyman continuum photons $N_{\rm Lyc}^{**}$ provided by the known OB stars from Table 1 is $1.43 \times 10^{50}$ $s^{-1}$ (Crowther 2005); the corresponding value for the nebula is $N_{\rm Lyc}^{\rm neb} \sim 2.4 \times 10^{50}$ $s^{-1}$ (Povich et al. 2007), scaled for the minimum distance of $d_{\rm min} = 2.0$ kpc. Using a distance of 2.1 kpc and the conversion by Crowther (2005) an equivalent of 11 O4 V stars is required to excite the nebula. Some of the "missing" early-type stars might exist in the form of spectroscopic binaries like e.g., CEN 1 a and b. Further early-type stars, sufficient to provide the ionization of the nebula, are suggested by the wealth of new photometry data. For example the nine X-ray sources in Figure 8 above the B0 reddening line are potential high-mass stars to be confirmed by future spectroscopy.

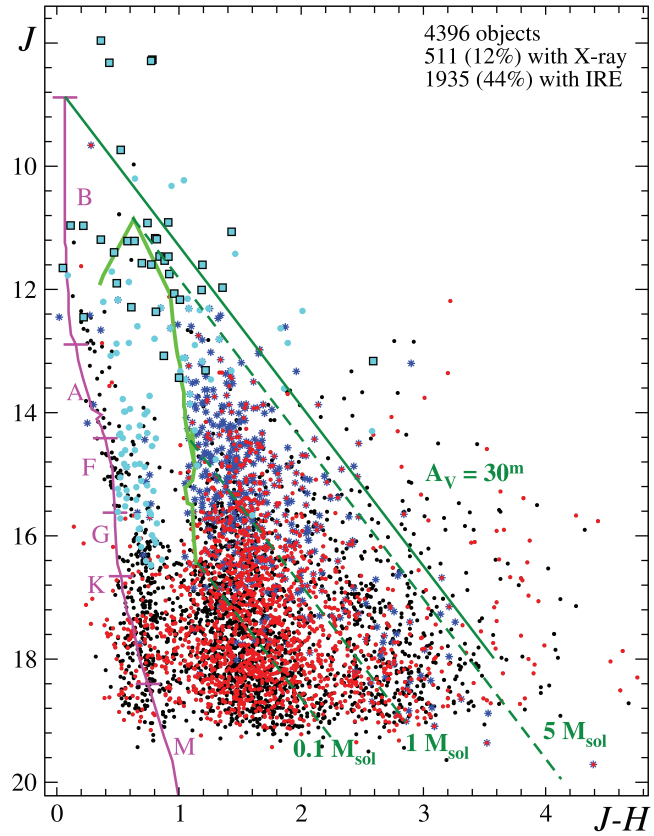


FIG. 8.—$J$ vs. $J - H$ color-magnitude diagram for 4396 stars. The solid magenta curve corresponds to the ZAMS for a distance of $d = 2.1$ kpc, corrected for a foreground extinction of $A_V = 2$ mag. Within the photometric accuracy it represents the lower left envelope of most data points; stars leftward of the ZAMS have extinctions less than 2 mag. The dashed light-green curve is a $5 \times 10^5$ yr isochrone (Siess et al. 2000) reddened by 4 mag. Loci of equal mass are indicated by the dashed green lines. The reddening vector, with a length of $A_V = 30$ mag, is shown as a solid green line; within the photometric accuracy this vector is independent of the extinction law. Cyan symbols refer to spectroscopically classified stars (*squares*: high-mass stars from Table 1; *filled circles*: intermediate- to low-mass stars). Blue asterisks characterize 511 (12%) stars with X-ray emission; red symbols denote 1935 (44%) stars with IRE. The diagram includes only data points with photometric errors less than 0.1 mag at each wave band.

### 5.5. *Low-Mass Stars*

The first detections of low-mass stars in M17 were reported by Broos et al. (2007). With the assumptions of $d = 1.6$ kpc and an age of 1 Myr, the majority of ACIS objects appear to be G and F stars ($0.5\ M_\odot < M < 2\ M_\odot$) reddened by about 3–15 mag of visual extinction. Correcting for the difference between 1.6 and 2.1 kpc shifts these stars more into the F–A regime. Figure 8 shows the position of the X-ray sources in the context of the results of the present paper, i.e., for a distance of 2.1 kpc and a foreground extinction of 2 mag.

As obvious from Figure 8 dereddened spectral types deviate significantly depending whether the stars are shifted onto the ZAMS or onto an isochrone with younger age. The scenario of triggered or sequential star formation, often discussed for M17 (§ 6), predicts stellar populations of various ages. As suggested by the gap in Figure 8 and emphasized by the isochrone, we adopt two populations of stars, one of which has an age of about 500,000 yr (see also § 5.7). If true, the low- to intermediate-mass X-ray sources span a range from 0.1 to 5 $M_\odot$.

Figure 8 provides further evidence for low-mass stars: Below $J \sim 16$, a large number of IRE objects become visible. If shifted back onto the ZAMS the majority of them would end up as G- or K-type stars. If they should turn out to be PMS stars, i.e., if they belong to the 500,000 yr population, their masses fall even below 0.1 $M_\odot$.

As discussed by Hoffmeister et al. (2006), IR spectroscopy is not particular helpful in M17 because the photospheres of most stars do not show any spectral features; this is most likely due to veiling by circumstellar dust. Our optical spectra for about 300 stars identifies a large number of potential cluster members ($A_V > 2$ mag) with intermediate- and low-mass types between A and M, many of which are located far above the ZAMS (Fig. 6).

### 5.6. *Circumstellar Disks*

First evidence for the presence of IRE objects in M17 was reported by Chini (1982) and Chini & Krügel (1985). The IR emission was interpreted as arising in cocoons (or tori) of circumstellar dust with temperatures of several 100 K. Chini & Wargau (1998) enlarged the number of IRE sources considerably by observations from 1.2 to 4.8 $\mu$m.

Lada et al. (1991) found that most OB stars (107) identified as cluster members in their M17 *JHK* study displayed IRE. Due to the fact that Lada et al. give neither a finding chart nor a table with photometric results, a direct comparison with other studies is not possible. In view of the results of the present paper, however, an IRE frequency of close to 100% for the OB stars in M17 can definitely be excluded. To check the results by Lada et al. (1991) we have investigated all stars with $K < 12.8$ inside the circular field observed by (Lada et al. 1991); among 510 stars in the *JHK* diagram we find 136 sources with IRE. Thus, the corresponding IRE frequency is only 27%.

The *JHK* color-color diagram presented by Hanson et al. (1997) includes 73 stars in a $6' \times 6.2'$. field with about 30% of them within the IRE region. Due to the fact that the photometry by Hanson et al. was obtained in a 3.6$''$ aperture, contamination from nearby stars seems to be a problem in the crowded cluster field; Lada et al. (1991) concluded that contribution from neighboring stars became a problem if the aperture was larger than 2.4$''$.

Jiang et al. (2002) also made the attempt to describe the YSOs with IRE by dividing them into two groups—454 Class I sources and 2798 Class II/Class III sources. This classification was based on the *JHK* color-color diagram (their Fig. 4*b*): stars in the reddened "T Tauri region," as outlined by the red line and the dashed reddening vector in Figure 3, were regarded as Class II/III, while stars located to the right of the dashed line were classified as Class I. Jiang et al. find that the Class II/Class III candidates are distributed all over the field, while Class I candidates occur generally in the H II region. The latter result cannot be retraced from the data given in the paper. First, their Table 2 lists 454 Class I sources in "M17" but only 235 are contained in the subregions 1C (20), 1S (97), 1N (115), and 2C (3). Second, Figure 10 of Jiang et al., which displays the spatial distribution of the Class I sources, contains 287 stars, most of which are located in the southern and northern bar. Therefore, a comparison with the present results cannot be made.

In order to compare the excess frequency of the M17 cluster with other young clusters, we performed the same procedure as described by Haisch et al. (2001a). As mentioned above, at $L = 13$ the detection rate is uniform over the entire field. Due to the higher sensitivity at *JHK* this limit holds for the remaining wave bands too. Selecting only stars brighter than $K = L = 13$ to be sensitive to stellar photospheres (i.e., $K - L \sim 0$) reveals a total of 496 stars equivalent to ZAMS spectral types of A4 or earlier. Among these there are 308 with IRE, thus leading to an excess frequency of 62% in M17. This number is remarkable in several aspects. First, it only refers to intermediate- and high-mass stars earlier than A4, which is unusual in comparison to the other young clusters (see below). Second, Figure 4 shows that the total number of stars with IRE increases toward lower masses: indeed, 1001 stars with $K$ and $L > 13$ yield an (incomplete) IRE frequency of >75%. In total, the combined IRE frequency is at least 74%.

Haisch et al. (2000) suggest that disks form around the majority of the stars in very young clusters *independent of mass*. Looking in detail into the data of the youngest clusters, however, it seems that the disk fraction is a function of spectral type.

As inferred from the $J$ vs. $J - H$ color-magnitude diagrams constructed from Table 2 in Haisch et al., NGC 2024 contains stars between O and G. The excess frequency as a function of spectral type is 58% (O, B), 69% (A), 76% (F), and 90% (G), i.e., it increases steadily with spectral type. Lada et al. (2000) also claim a mass independence for the Trapezium cluster. There the excess frequencies increase from 42% (12 O, B, A) to 78% (9 F, G), 82% (87 K), and 81% (177 M); for 62 substellar sources the occurrence of IRE decreases to 50%. Finally, Haisch et al. (2001a) found in IC 348 9 stars of spectral types O, B, A, and F that appear diskless, while 6 G, 23 K, and 42 M stars have a disk fraction of 50%, 52%, and 67%, respectively. Thus, in summary, there is a correlation between increasing IRE frequency and spectral type, with the OBA types having the lowest IRE fractions.

From the formal estimates given above, it seems that M17 belongs to those young clusters with the highest disk frequency for high- and intermediate-mass stars. In this respect it is comparable to NGC 2024. On the other hand, IR excess in early-type stars cannot be interpreted as necessarily indicating a circumstellar disk, since a small amount of dust relatively far away from an OB star can still cause a huge excess due to the prodigious radiative heating present. Chini & Krügel (1985) have shown that a dust mass equivalent to $A_V = 0.1$ mag produces excess emission of several magnitudes above the stellar photosphere in the range 1–4 $\mu$m. Given, however, that some disks around O- and B-type stars in M17 have been directly imaged (Chini et al. 2006; Nielbock et al. 2007), we believe that most IR excesses are due to genuine circumstellar material.

### 5.7. *Cluster Age*

It is difficult to gauge the age of the youngest star clusters by comparing stellar loci in color-magnitude diagrams with evolutionary tracks. This procedure requires precise knowledge of spectral type, reddening, and brightness, which is hard to achieve simultaneously for deeply embedded YSOs. Moreover, it is far from clear whether the ignition of SF in a molecular cloud is coeval for high- and low-mass stars; sequential SF complicates the situation in a large stellar aggregate.

Despite these caveats, we interpret the gap in Figure 8 in terms of stellar evolution and suggest the presence of at least two populations of stars: (1) Stars on (or close to) the ZAMS, which include most of the exciting stars in the region originating from a first episode of SF in M17. They have cleared the ISM in their surroundings and thus suffer from only moderate extinction ($A_V =$ 1–3 mag). (2) Stars beyond the gap are likely due to a second SF epoch and are embedded more deeply into the area. As demonstrated by Figures 5*d*–5*f*, however, they are not associated with cloud B but occur predominantly toward the H II region, like the less reddened stars. Figure 8 shows an isochrone of $5 \times 10^5$ yr (Siess et al. 2000) reddened by 4 mag of extinction which serves

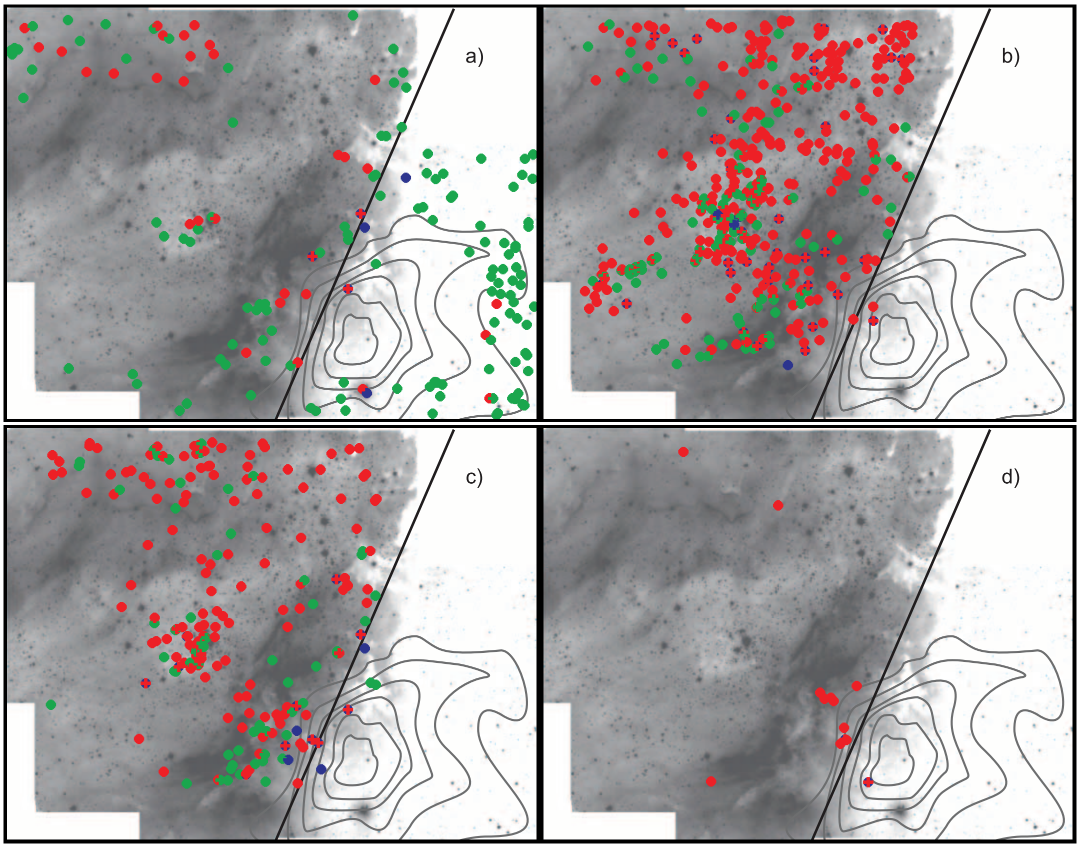


FIG. 9.—Distribution of extremely red objects. (*a*) 158 sources with $H - K > 2.4$; (*b*) 423 sources with $1.5 \leq K - L < 2.0$; (*c*) 211 sources with $2.0 \leq K - L < 4.0$; (*d*) 13 sources with $K - L \geq 4.0$. Red symbols correspond to IRE objects and blue symbols denote X-ray sources; green dots are normal stars without X-ray emission or IRE. The straight line crudely separates the nebular region from the southwestern molecular cloud, which is denoted by the gray $C^{18}O$ contours adapted from Wilson et al. (2003).

as a lower left envelope for most stars beyond the gap. If true, this would mean that at least a second episode of SF has occurred in the region.

As an alternative approach one can use the timescale for circumstellar disk dissipation as an indirect probe for the age of a cluster. Haisch et al. (2001a) discuss the lifetimes of circumstellar disks, based on six young clusters that span a range in age of 0.3 to 30 Myr; the corresponding disk fractions started at 3% ± 3% for NGC 1960 (30 Myr) and increased to 80% ± 5% for the 1.5 Myr old Trapezium cluster and to 85% ± 8% for NGC 2024 (0.3 Myr). Analysis indicates that the cluster disk fraction rapidly decreases with increasing cluster age, such that one-half the stars in the clusters lose their disks in ≲3 Myr. As outlined in § 5.6, the frequency of disks in M17 is 62% for stars earlier than A4 and increases to more than 75% for later spectral types. This disk frequency places M17 among the youngest galactic aggregates, such as NGC 2024, and argues in favor of a lifetime less than 500,000 yr for the youngest generation of stars.

Obviously, such estimates depend on the method of detecting disks, i.e., generally via *K*- or *L*-band excess for ground-based observations or MIR excess as accessible from satellites. Therefore, studies that determine disk frequencies as a function of cluster age have to be compared with caution, depending on how the excess was observed; the influence of intrinsic colors and reddening law has been discussed above. In addition, a high abundance of nearby O stars might decrease the lifetime of disks considerably.

### 5.8. *Extremely Red Objects*

Chini (1982) and Chini & Krügel (1985) found seven early B-type stars and one unknown source, whose SED between 0.3 and 20 $\mu$m displayed the largest IREs known for optically visible stars at that time. These objects were interpreted as "cocoon stars" with shells or tori of dust of several 100 K. Giard et al. (1994) presented among others *K*- and *L*-band images of the Arc region. In their Table 1, seven extremely red ($K - L > 3.5$) sources—different from those of Chini & Krügel (1985)—were listed, among them M17-UC1 and IRS 5. The red colors led Giard et al. (1994) to conclude that this group is in a very early evolutionary stage. Our photometry corroborates the conclusion that these sources are fairly red, although the *K* and *L* brightness for individual objects differs by more than 2 mag in certain cases. Whether this result is due to variability has to await further observations.

Jiang et al. (2002) also discussed a group of very red sources ($H - K \geq 2.4$) for which they could not obtain *J*-band data. They argue that the majority of these red sources should be YSOs with intrinsic IRE associated with the molecular clouds surrounding the H II region (Fig. 5 of Jiang et al. ). Our data—although referring to a smaller field—do not corroborate this interpretation. Figure 9 a shows the spatial distribution of 158 sources with $H - K > 2.4$ half of which are concentrated southwest of cloud B. Our *JHKL* data, however, reveal that this red population contains only 21% IRE objects and 2% X-ray emitters, indicating that the majority is not particularly young with intrinsic IRE. Moreover, the few sources with IRE and X-ray emission in this sample seem to be associated with the H II region and not with the molecular cloud. In fact, there are only three stars with IRE—apart from the Kleinmann-Wright object—outside the H II region. This makes it rather likely that the sources toward the molecular cloud are unrelated background sources shining through the southwestern edge of cloud B.

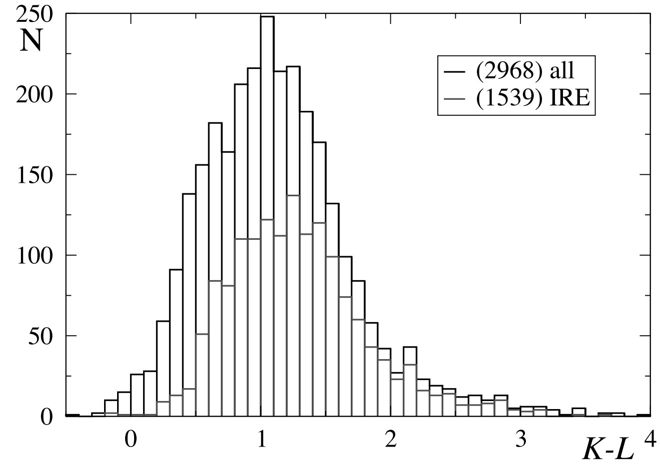


FIG. 10.—$K - L$ color distribution of extremely red objects. Thirteen sources with $4 < K - L < 7$ are not included. The IRE for 1361 objects (88%) has been determined from the *HKL* diagram in Fig. 4; the remaining 178 IRE sources come from the *JHK* diagram in Fig. 3. [*See the electronic edition of the Journal for a color version of this figure.*]

Our IR database contains a large number of red objects too; more than half of about 3000 sources in M17 with detections at $K$ and $L$ have colors $K - L > 1.1$, with a dozen of sources characterized by extremely red colors of $4 < K - L < 7$. As discussed above, variability between the different epochs for the *JHK* and the $L$ observations could contaminate some of the $K - L$ colors. Given, however, that there are only extremely red and no unusually "blue" sources, the $K - L$ colors seem to be fairly reliable.

If the $K - L$ values of these extremely red sources are due to pure reddening by dust this would imply extinctions $A_V$ of up to 160 mag. Such extreme extinctions typically arise from dense disks or envelopes of deeply embedded protostellar objects and not from the more diffuse dust of a molecular cloud core. If, on the other hand, these red colors are caused by strong IRE emission, the sources also must be protostellar in nature and still in the process of forming.

To discriminate between extinction and IRE, these red sources have been examined in the $H - K$ vs. $K - L$ diagram. Figure 10 shows the distribution of $K - L$ colors for 2968 stars of which 52% have IRE. The peak for all sources lies at $K - L \sim 1.1$ mag; the peak for IRE sources is slightly shifted to $K - L \sim 1.3$. In general, the IRE frequency increases with $K - L$. There are 647 objects with $K - L \geq 1.5$. Within the range $1.5 \leq K - L < 2.0$ there are 423 sources of which 77% lie within the IRE region. Among 211 sources with $2.0 \leq K - L < 4.0$ the excess fraction is even 89%. All (13) objects with $K - L \geq 4$ have IRE. Thus, it seems that large IREs are responsible for the red colors. The statistics for these red sources are summarized in Table 3.

To put this extremely red population of M17 in context, it is helpful to compare it with other young clusters. In the Taurus population of YSOs, sources with $K - L > 0.4$ were classified to have *substantial* IRE; objects with $K - L \sim 1.5$ mag were even regarded as *protostellar* in nature (Kenyon & Hartmann 1995). In NGC 2024 a broad peak, centered around $K - L \simeq 0.8 - 1.0$, appeared in the color distribution, with only a small fraction of the sources having $K - L \geq 2.0$ (Haisch et al. 2000). Four sources have $K - L \geq 4.0$, including one source which was detected only at $L$. In analogy to Taurus, Haisch et al. suggested that 45 sources with $K - L \geq 1.5$ are Class I (i.e., protostellar) objects. In the Trapezium cluster (Lada et al. 2000) the color distribution of 603 stars detected in $K$ and $L$ has a broad but prominent peak at $K - L \sim 0.9$ mag, very similar to that in NGC 2024. Lada et al. attribute the shift of the peak to relatively large $K - L$ color primarily to infrared excess emission and to a lesser extent to reddening. It would require about 25 mag of visual extinction to produce a $K - L$ color of 1.0 mag in a naked, diskless star, but examination of the Trapezium color-color diagrams shows that the vast majority of stars in the cluster have extinctions well under $A_V = 10$ mag. As a consequence, Lada et al. identify 78 candidate protostars from their list of sources with $K - L$ colors in excess of 1.5 mag. NGC 3603 contains only 117 IRE objects with $K - L$ generally below 2.0 (Stolte et al. 2004). Finally, in IC 348 there exists no source at all with $K - L > 1.5$ (Haisch et al. 2001b). Thus, the red population in M17 is the largest one detected in a young cluster so far; simultaneously, it displays the reddest $K - L$ colors.

The spatial distribution of these extremely red sources is displayed in Figures 9*b*–9*d*. The group $1.5 \leq K - L < 2.0$ occurs predominantly in the central cluster and its northwestern extension; further sources are scattered in the northern and southwestern bar (Fig. 9*b*). Sources with $2 \leq K - L < 4$ show faint concentrations in the cluster center as well as along the northern bar and southwestern bar (Fig. 9*c*). Most of the reddest sources ($K - L > 4$) are located in the arc region and southwest of it (Fig. 9*d*)—among them M17-UC1 ($K - L \sim 6.6$) and the maser source associated with IRS 5 ($K - L \sim 4.2$). Another red source ($K - L \sim 5.2$) emerges at the tip of a large trunk in the northwest pointing toward CEN 1.

## 6. SEQUENTIAL STAR FORMATION

Elmegreen & Lada (1977) have presented a scheme in which subgroups of OB associations drive ionization-front shocks into molecular clouds to trigger the formation of new subgroups. As a consequence one should be able to observe an age gradient along the propagation of the star-forming process with loose OB associations at the "old" end and YSOs or protostellar sources at the "young" end. Quantitatively, there should be signpost of recent SF in the molecular cloud within 10–15 pc of the nearest OB stars. Elmegreen et al. (1979) have suggested that M17 SW is one of those clouds in which sequential star formation is under way. However, Jaffe & Fazio (1982) found no evidence for an age gradient along the ~160 pc extent of M17 SW. The almost

TABLE 3
STATISTICS OF EXTREMELY RED SOURCES

| | H II REGION ($N$ = 88/638) | | | CLOUD B ($N$ = 70/9) | | |
|---|---|---|---|---|---|---|
| COLOR | Normal | IRE | X-ray | Normal | IRE | X-ray |
| $H - K > 2.4$ | 59 (37%) | 28 (18%) | 3 (2%) | 63 (40%) | 5 (3%) | 3 (2%) |
| $1.5 \leq K - L < 2.0$ | 103 (24%) | 314 (74%) | 39 (9%) | 0 (0%) | 2 (0.5%) | 1 (0.2%) |
| $2.0 \leq K - L < 4.0$ | 60 (28%) | 143 (68%) | 11 (5%) | 2 (1%) | 2 (1%) | 4 (2%) |
| $K - L \geq 4.0$ | 0 (0%) | 12 (92%) | 1 (8%) | 0 (0%) | 1 (8%) | 1 (8%) |

regular distribution of compact FIR sources and $H_2O$ masers suggests that these signposts for recent SF are entirely unrelated to the nearby giant H II region and more likely a result of a global spiral shock. Likewise, the study by Elmegreen et al. (1988) yielded no indication for any age gradient along the cloud.

Our *JHKL* survey has covered a small portion ($\sim$25 arcmin$^2$) of the molecular cloud southwest of M17-UC1. Among the 226 NIR sources detected in this area there are 56 (25%) IRE sources and 6 (2%) X-ray emitters (see Table 2). The relative abundances of these youth signatures are significantly below the values of the central cluster and support the idea that SF occurs in all parts of the cloud–independent of the influence by the H II region.

If there exists triggered star formation in the M17 complex, then it occurs on much smaller scales, i.e., at the interface of the H II region with the molecular cloud. The prominent young high-mass objects M17-UC1 and IRS 5 and the KW object, as well as other sources such as B 273 or CEN 92 (Hoffmeister et al. 2006), likely represent a spatially distinct and more recent phase of star formation in the southern bar than the central OB cluster. Likewise, the occurrence of protostars in Figures 9*c* and 9*d* suggests that the youngest sources are not uniformly distributed across the region. This might be interpreted as locally triggered SF by the central O stars in the central cluster.

## 7. CONCLUSIONS

Multicolor photometry and spectroscopy of the M17 cluster has led to the following results:

1. A spectrophotometric distance of $2.1 \pm 0.2$ kpc has been obtained from 53 OB stars. This value is compatible with the kinematic distance and excludes earlier determinations, which were significantly below 2 kpc.

2. The number of newly identified OB stars and high-mass candidates is sufficient to provide the excitation of the H II region. Multiplicity of several O stars could be established, among them the two major exciting O4 stars in the cluster center.

3. The optical extinction law is characterized by $R = 3.9 \pm 0.2$. The foreground extinction toward M17 is $A_V \sim 2$ mag and allows us to distinguish unrelated field stars from stars inside the H II region. Likewise, the high extinction of up to 40 mag produced by the dust inside the H II region exclude contamination by unrelated background stars.

4. Within a projected area of $3.6 \times 3.7$ pc, there are several thousand stars which have been identified as cluster members on the basis of their extinction, X-ray emission, and IR excess.

5. The excess frequency for stars earlier than A4 is 62% and increases to about 74% for fainter stars. Most of the excess emission is probably due to circumstellar disks. In the case of high-mass stars small amounts of hot dust somewhere near the stars could also produce an IR excess. Nevertheless, the presence of dust in the vicinity of many high-mass stars argues in favor of the extreme youth of the cluster.

6. Various arguments support a scenario of sequential star formation: There about 500 moderately reddened sources on the ZAMS, among them many OB stars. About 3350 heavily reddened sources are most likely deeply embedded pre-main-sequence objects with an age of less than $5 \times 10^5$ yr. A group of 647 accreting protostellar candidates has been detected in the periphery of the cluster and argues in favor of ongoing star formation triggered by the central O stars in M17.

In the first place we wish thank our anonymous referee for detailed and constructive remarks which improved the paper considerably. We also thank the VLT team for performing the *JHKL* observations in service mode. N. V. acknowledges support by FONDECYT grant 1061199 and by UCN grant DGIP-10301180. This work was partly funded by the Nordrhein-Westfälische Akademie der Wissenschaften.

*Facilities:* VLT:Antu (ISAAC), NTT (EMMI), VLT:Kueyen (FLAMES)

## REFERENCES

Anderson, C. M. 1970, ApJ, 160, 507
Ando, M., Nagata, T., Sato, S., Mizuno, N., Mizuno, A., Kawai, T., Nakaya, H., & Glass, I. S. 2002, ApJ, 574, 187
Bagnulo, S., et al. (ESO Paranal Science Operations Team). 2003, Messenger, 114, 10
Bahcall, J. N., & Soneira, R. M. 1980, ApJS, 44, 73
Beetz, M., Elsässer, H., Weinberger, R., & Poulakos, C. 1976, A&A, 50, 41
Bessell, M. S., & Brett, J. M. 1988, PASP, 100, 1134
Broos, P. S., Feigelson, E. D., Townsley, L. K., Getman, K. V., Wang, J., Garmire, G. P., Jiang, Z., & Tsuboi, Y. 2007, ApJS, 169, 353
Cardelli, J. A., Clayton, G. C., & Mathis, J. S. 1989, ApJ, 345, 245
Chini, R. 1982, A&A, 110, 332
Chini, R., Elsässer, H., & Neckel, T. 1980, A&A, 91, 186 (CEN80)
Chini, R., Hoffmeister, V. H., Nielbock, M., Scheyda, C. M., Steinacker, J., Siebenmorgen, R., & Nürnberger, D. 2006, ApJ, 645, L61
Chini, R., & Krügel, E. 1983, A&A, 117, 289
———. 1985, A&A, 146, 175
Chini, R., & Wargau, W. F. 1998, A&A, 329, 161
Crampton, D., Georgelin, Y. M., & Georgelin, Y. P. 1978, A&A, 66, 1
Crowther, P. A. 2005, in IAU Symp. 227, Massive Star Birth, ed. R. Cesaroni, M. Felli, E. Churchwell, & M. Walmsley (Cambridge: Cambridge Univ. Press), 389
Dekker, H., Delabre, B., & Dodorico, S. 1986, in Instrumentation in Astronomy VI, ed. D. L. Crawford (Bellingham, WA: SPIE), 339
Dickel, H. R. 1968, ApJ, 152, 651
Ducati, J. R., Bevilacqua, C. M., Rembold, S. B., & Ribeiro, D. 2001, ApJ, 558, 309
Elmegreen, B. G., & Lada, C. J. 1977, ApJ, 214, 725
Elmegreen, B. G., Lada, C. J., & Dickinson, D. F. 1979, ApJ, 230, 415
Elmegreen, D. M., Phillips, J., Beck, K., Thomas, H., & Howard, J. 1988, ApJ, 335, 803
Felli, M., Churchwell, E., & Massi, M. 1984, A&A, 136, 53
Fitzpatrick, E. L. 1999, PASP, 111, 63
Giard, M., Bernard, J. P., Lacombe, F., Normand, P., & Rouan, D. 1994, A&A, 291, 239
Glushkov, Y. I., Esipov, V. F., & Kondrat'Eva, L. N. 2005, Astron. Rep., 49, 36
Haisch, K. E., Lada, E. A., & Lada, C. J. 2000, AJ, 120, 1396
———. 2001a, ApJ, 553, L153
———. 2001b, AJ, 121, 2065
Hanson, M. M., Howarth, I. D., & Conti, P. S. 1997, ApJ, 489, 698
Hoffmeister, V. H., Chini, R., Scheyda, C. M., Nürnberger, D., Vogt, N., & Nielbock, M. 2006, A&A, 457, L29
Ishida, K., & Kawajiri, K. 1968, PASJ, 20, 95
Jaffe, D. T., & Fazio, G. G. 1982, ApJ, 257, L77
Jiang, Z., et al. 2002, ApJ, 577, 245
Johnson, H. L., & Hiltner, W. A. 1956, ApJ, 123, 267
Jones, T. J., & Hyland, A. R. 1980, MNRAS, 192, 359
Kenyon, S. J., & Hartmann, L. W. 1995, ApJS, 101, 117
Kenyon, S. J., Lada, E. A., & Barsony, M. 1998, AJ, 115, 252
Kleinmann, D. E. 1973, Astrophys. Lett., 13, 49
Lada, C. J., Depoy, D. L., Merrill, K. M., & Gatley, I. 1991, ApJ, 374, 533
Lada, C. J., Muench, A. A., Haisch, K. E., Jr., Lada, E. A., Alves, J. F., Tollestrup, E. V., & Willner, S. P. 2000, AJ, 120, 3162
Landolt, A. U. 1992, AJ, 104, 340
Meyer, M. R., Calvet, N., & Hillenbrand, L. A. 1997, AJ, 114, 288
Moorwood, A., et al. 1998, Messenger, 94, 7
Nagata, T., Hyland, A. R., Straw, S. M., Sato, S., & Kawara, K. 1993, ApJ, 406, 501
Naoi, T., et al. 2006, ApJ, 640, 373
Nielbock, M., Chini, R., Hoffmeister, V. H., Scheyda, C. M., Steinacker, J., Nürnberger, D., & Siebenmorgen, R. 2007, ApJ, 656, L81
Nielbock, M., Chini, R., Jütte, M. Manthey, E. 2001, A&A, 377, 273

Ogura, K., & Ishida, K. 1976, PASJ, 28, 35
Pasquini, L., et al. 2002, Messenger, 110, 1
Persson, S. E., Murphy, D. C., Krzeminski, W., Roth, M., & Rieke, M. J. 1998, AJ, 116, 2475
Povich, M. S., et al. 2007, ApJ, 660, 346
Pronik, I. I. 1958, Izv. Krymskoi Astrofiz. Obs., 20, 208
Rousselot, P., Lidman, C., Cuby, J.-G., Moreels, G., & Monnet, G. 2000, A&A, 354, 1134
Russeil, D. 2003, A&A, 397, 133
Schmidt-Kaler, Th. 1982, Stars and Star Clusters, ed. K. Schaifers, H. H. Voight, & H. Landolt (Landolt-Börnstein New Series, Group 6, Vol. 2C; Berlin: Springer)
Schulte, D. H. 1956, ApJ, 123, 250
Siess, L., Dufour, E., & Forestini, M. 2000, A&A, 358, 593
Silva, D. R., & Cornell, M. E. 1992, ApJS, 81, 865
Stephenson, C. B., & Hobbs, R. W. 1961, AJ, 66, 186
Stolte, A., Brandner, W., Brandl, B., Zinnecker, H., & Grebel, E. 2004, AJ, 128, 765
Strom, K. M., Strom, S. E., Edwards, S., Cabrit, S., & Skrutski, M. F. 1989, AJ, 97, 1451
Wilson, T. L., Hanson, M. M., & Muders, D. 2003, ApJ, 590, 895